

# Calibrating the Baryon Oscillation Ruler for Matter and Halos

Nikhil Padmanabhan<sup>1,\*</sup> and Martin White<sup>2,†</sup>

<sup>1</sup>*Physics Division, Lawrence Berkeley National Laboratory, 1 Cyclotron Rd., Berkeley, CA 94720*

<sup>2</sup>*Departments of Physics and Astronomy, 601 Campbell Hall, University of California Berkeley, CA 94720*

*Physics Division, Lawrence Berkeley National Laboratory, 1 Cyclotron Rd., Berkeley, CA 94720*

(Dated: November 8, 2018)

We characterize the nonlinear evolution of the baryon acoustic feature as traced by the dark matter and halos, using a combination of perturbation theory and N-body simulations. We confirm that the acoustic peak traced by the dark matter is both broadened and shifted as structure forms, and that this shift is well described by second-order perturbation theory. These shifts persist for dark matter halos, and are a simple function of halo bias, with the shift (mostly) increasing with increasing bias. Extending our perturbation theory results to halos with simple two parameter bias models (both in Lagrangian and Eulerian space) quantitatively explains the observed shifts. In particular, we demonstrate that there are additional terms that contribute to the shift that are absent for the matter. At  $z = 0$  for currently favored cosmologies, the matter shows shifts of  $\sim 0.5\%$ ,  $b = 1$  halos shift the acoustic scale by  $\sim 0.2\%$ , while  $b = 2$  halos shift it by  $\sim 0.5\%$ ; these shifts decrease by the square of the growth factor  $D(z)$  at higher redshifts. These results are easily generalized to galaxies within the halo model, where we show that simple galaxy models show marginally larger shifts than the correspondingly biased halos, due to the contribution of satellites in high mass halos. While our focus here is on real space, our results make specific predictions for redshift space. For currently favored cosmological models, we find that the shifts for halos at  $z = 0$  increase by  $\sim 0.3\%$ ; at high  $z$ , they increase by  $\sim 0.5\% D^2$ . Our results demonstrate that these theoretical systematics are smaller than the statistical precision of upcoming surveys, even if one ignored the corrections discussed here. Simple modeling, along the lines discussed here, has the potential to reduce these systematics to below the levels of cosmic variance limited surveys.

PACS numbers: 95.36.+x,98.80.-k

## I. INTRODUCTION

It has been known for many years that the coupling of photons and baryons in the early universe results in an almost harmonic series of oscillations in the matter power spectrum [1, 2, 3] with a scale set by the sound horizon,  $s \sim 100$  Mpc (see [4, 5] for a detailed description of the physics in modern cosmologies and [6] for a comparison of Fourier and configuration space pictures). This feature can be used as a ‘standard ruler’ to measure the expansion rate of the Universe, and this baryon acoustic oscillation (BAO) method is an integral part of current and next-generation dark energy experiments.

While the early Universe physics is linear and well understood, the low redshift observations are complicated by the nonlinear evolution of matter and the non-trivial relation between galaxies and dark matter. The nonlinear evolution leads to a damping of the oscillations on small scales [5, 6, 7, 8, 9, 10, 11] and the generation of a small out-of-phase component [6, 9, 10, 11, 12, 13]. The damping of the linear power spectrum (or equivalently the smoothing of the correlation function) reduces the contrast of the feature and thereby the precision with which the size of ruler may be measured. The out-of-phase component corresponds to a shift in the acoustic scale which would bias the distance measure if it were not taken into account.

In this paper we investigate the behavior of the acoustic signal in biased tracers of the nonlinear mass field. We find that

biased tracers have different shifts than the matter, and discuss how these shifts can be modeled and significantly reduced.

## II. PRELIMINARIES

One of the challenges of calibrating systematic effects in BAO is the very large scale of the acoustic feature, which requires huge volumes to be surveyed/simulated and reduces the effects of nonlinearities and astrophysical uncertainties. While the latter is what makes BAO an attractive standard ruler, the combination makes it challenging to measure systematics with any statistical precision. To avoid these issues, we start with a toy cosmology ( $\epsilon$ CDM, see also [16]) which has  $\Omega_M = 1$ ,  $\Omega_B = 0.4$ ,  $h = 0.5$ ,  $n = 1$  and  $\sigma_8 = 1$ . This cosmology has an unrealistically high baryon fraction, a much smaller acoustic oscillation scale ( $\sim 50 h^{-1}$  Mpc compared with the  $\sim 100 h^{-1}$  Mpc of the ‘concordance’ cosmology) and is more nonlinear at  $z = 0$  than our Universe is believed to be. This emphasizes the effects we are investigating while reducing the sampling error, simplifying the numerical problem and allowing us to obtain highly robust measures of small effects. In § V, we extend the model constructed to concordance  $\Lambda$ CDM cosmologies, focusing on one with  $\Omega_M = 0.25$ ,  $\Omega_B h^2 = 0.0224$ ,  $h = 0.72$ ,  $n_s = 0.97$  and  $\sigma_8 = 0.8$  for definiteness.

To model nonlinear structure formation and the formation of dark matter halos we used 10 independent simulations each of  $1024^3$  particles in periodic, cubical boxes of side length  $2 h^{-1}$  Gpc. The simulations were started at  $z = 100$  using the Zel’dovich approximation and evolved to  $z = 0$  with the TreePM [17] code. The full phase-space data were dumped at

\*Electronic address: NPadmanabhan@lbl.gov

†Electronic address: mwhite@berkeley.edu

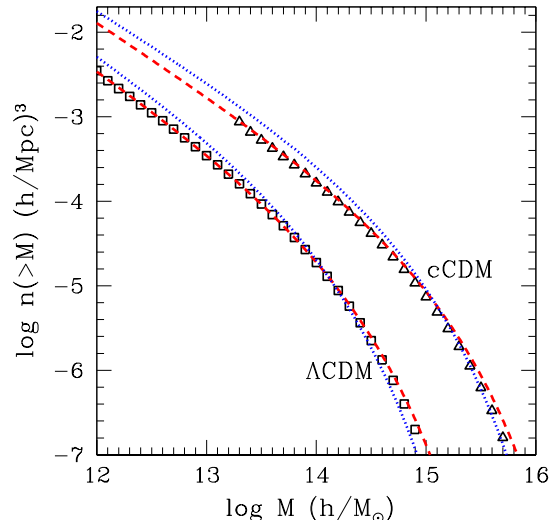


FIG. 1: The mass functions at  $z = 0$  for our  $c$ CDM (triangles) and  $\Lambda$ CDM (squares) cosmologies, along with two commonly used fitting functions due to Press & Schechter [14] (dotted, blue) and Sheth & Tormen [15] (dashed, red). Since we are using the sum of the particles in a FoF group for our definition of mass, we do not expect perfect agreement with either fitting function. The simulations for the  $\Lambda$ CDM cosmology are discussed in §V.

a number of redshifts between  $z = 1$  and  $z = 0$ , and groups were found using the friends-of-friends algorithm [18] with a linking length of 0.168 times the mean interparticle spacing. We keep all groups down to 10 particles, or  $2 \times 10^{13} h^{-1} M_{\odot}$ , using the sum of the particle masses in the group as our halo mass definition for simplicity. These minimum masses correspond to peak heights running from  $\nu \simeq 1$  at  $z = 0$  to  $\nu \simeq 2$  at  $z = 1$ . The mass function and nonlinear power spectrum for this model are shown in Figures 1 and 2 for reference. Throughout this paper we do not subtract shot-noise from the power spectra, but allow it to be a nuisance parameter in our fits (see below). More details on these simulations, including convergence tests, are in [16].

Fitting the acoustic scale involves locating the position of the acoustic feature while allowing for variations in the broad-band shape due to e.g. galaxy biasing. We do so by fitting the observed power spectra with

$$P_{\text{fit}}(k) = B(k)P_w(k, \alpha) + A(k), \quad (1)$$

where  $A(k)$  and  $B(k)$  are smooth functions and  $\alpha$  measures the acoustic scale relative to a “best-guess” cosmology.  $P_w$  is a template for the biased, nonlinear acoustic feature. This definition of peak “shift” is over and above the shift in the point where  $\xi'(r) = 0$ , or shifts in the extrema of the oscillations in the power spectrum. A good match between theory and observations, including the correct background cosmology and hence distance-redshift relation, should give  $\alpha \equiv 1$ .

Note that the precise partitioning into acoustic feature and broad band shape is dependent on the particular choices of  $A$  and  $B$ . Since constructing an accurate template for the acous-

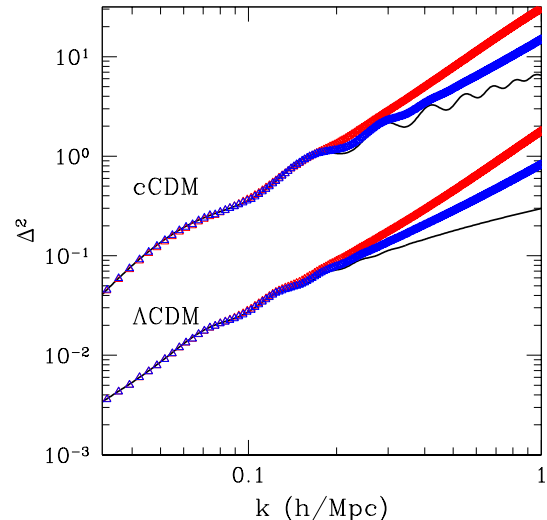


FIG. 2: The nonlinear matter power spectrum at  $z = 0$  (red, upper) and  $z = 1$  (blue, middle), compared to the linear theory (black, lower) for our  $c$ CDM and  $\Lambda$ CDM models. The  $z = 1$  power spectra have been scaled by  $1/D^2$  to match the other power spectra on large scales and the  $\Lambda$ CDM spectra have been offset (vertically) for clarity. Note the strong damping of the oscillations and the large excess power on small scales in the evolved fields.

tic feature yields a good template for larger scales, we assume  $B(k)$  is a constant.  $A(k)$  is assumed to be a cubic spline specified at 0.0, 0.1,  $\dots$ , 0.4 and derivatives specified at the end points. The shot noise component is simply absorbed into  $A(k)$ . The above prescription yields seven nuisance parameters; we do not vary this (or the particular prescription) in this paper, although we do get consistent results for different choices.

The fits are done by  $\chi^2$  minimization, fitting the 70 power spectrum bins between  $k = 0.02 h \text{Mpc}^{-1}$  and  $0.35 h \text{Mpc}^{-1}$ . We assume a diagonal covariance matrix where the errors are a smooth fit to the run to run variance of the 10 simulations. The errors on all derived quantities are determined the variance of 1,000 bootstrap resamplings.

We now turn to the purpose of this paper - the determination of  $P_w$ , first for the matter and then for biased tracers.

### III. MATTER

As is dramatically evident in Fig. 2, the sharp acoustic feature at high redshift gets smeared by bulk flows and supercluster formation as the Universe evolves [5, 6, 7, 8, 9, 10]. An estimate of the smearing is given by convolving the matter correlation function with a Gaussian of width equal to the rms displacement of particles from their initial positions. To lowest order this is the rms Zel’dovich displacement

$$\Sigma_1^2 = \frac{1}{3\pi^2} \int dk P_L(k) \quad (2)$$

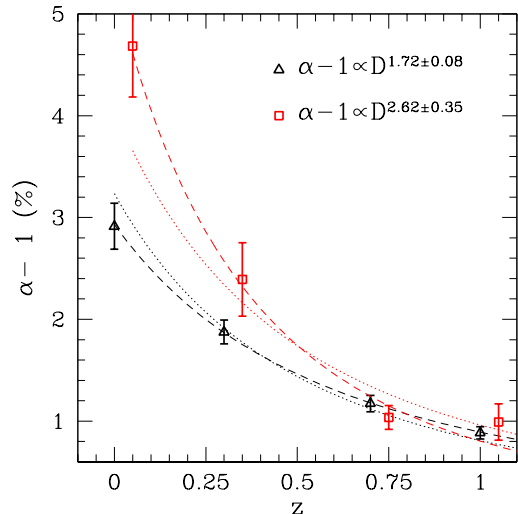


FIG. 3: The shift in the acoustic scale,  $\alpha - 1$  vs. redshift for the mass (black triangles) and  $\nu = 1.9$  halos (red squares) using Eq. (3) as the template. Also shown are the best fit power-laws (dashed) and the expectations of perturbation theory [ $\alpha - 1 \propto D^2(z)$ ] (dotted). The points and curves for the halos are shifted by  $\delta z = 0.05$  for clarity.

suggesting a template of the form

$$P_w(k, \alpha) = \exp\left(-\frac{k^2 \Sigma^2}{2}\right) P_L(k/\alpha) \quad (3)$$

where  $P_L$  is the linear theory power spectrum at the redshift of interest, and  $\Sigma$  is allowed to vary. The lowest order result is the same whether obtained using the peak-background split [6], renormalized perturbation theory [9] or resummed Lagrangian perturbation theory [10]. While the Gaussian form of the smearing is a reasonable approximation to what we see in the simulations, we find  $\mathcal{O}(10\%)$  deviations from  $\Sigma_1$  in our cosmology.

Figure 3 and Table I summarize the shifts obtained using the above template. We find that  $\alpha \neq 1$  at very high significance, with  $\alpha - 1 \sim 4\%$  at  $z = 0$ . We remind the reader that this is an extreme cosmology; the shifts for a concordance cosmology (as we discuss in §V) are approximately an order of magnitude smaller. We also observe that the shifts decrease with redshift as  $\alpha - 1 \sim D^2$  (adopting the convention  $D(z = 0) = 1$ ), consistent with the field getting more linear at higher redshift and suggestive that the next order terms in perturbation theory ( $\mathcal{O}(P_L^2)$ , see [16] for a recent review) are responsible (see also [9, 11] who emphasized this point).

To explore this possibility, we expand the density contrast in powers of linear density  $\delta_L$

$$\delta = \delta^{(1)} + \delta^{(2)} + \delta^{(3)} + \dots \quad (4)$$

with  $\delta^{(1)} \equiv \delta_L$ . It is straightforward to show that

$$\begin{aligned} \delta^{(n)}(k) &= \int \frac{d^3 q_1 \dots d^3 q_n}{(2\pi)^{3n}} (2\pi)^3 \delta_D\left(\sum q_i - k\right) \\ &\times F_n(\{q_i\}, k) \delta_L(q_1) \dots \delta_L(q_n) \end{aligned} \quad (5)$$

| $z$ | DM              | $x\delta_L$      | w/ $P_{22}$      |
|-----|-----------------|------------------|------------------|
| 0.0 | $2.91 \pm 0.20$ | $-0.19 \pm 0.08$ | $-0.03 \pm 0.16$ |
| 0.3 | $1.88 \pm 0.12$ | $-0.18 \pm 0.11$ | $-0.38 \pm 0.09$ |
| 0.7 | $1.17 \pm 0.07$ | $-0.13 \pm 0.11$ | $-0.12 \pm 0.05$ |
| 1.0 | $0.88 \pm 0.06$ | $-0.11 \pm 0.12$ | $-0.04 \pm 0.04$ |

TABLE I: Shifts, i.e.  $\alpha - 1$  in per cent, for the matter density autopower spectrum and the cross-spectrum of the density with the linearly extrapolated initial density field. The presence of a shift in the first column and not in the second demonstrates that the shifts arise from the higher order  $P_{mn}$  ( $m, n \geq 2$ ) contributions to the power spectrum (see text for details). The last column demonstrates that this shift can be corrected by adding a  $P_{22}$  term to the template.

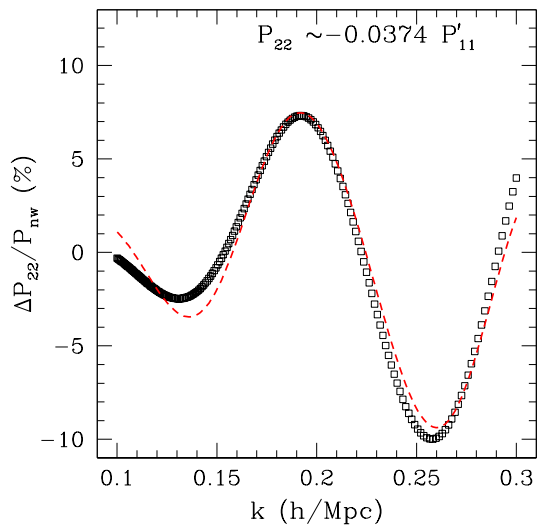


FIG. 4: The out-of-phase contribution predicted by perturbation theory well approximates the derivative of the acoustic signal. The points plot  $P_{22}$ , while the line is a scaled version of  $dP_L/d \ln k$  with the scaling given in the inset. The smooth components of both curves have been subtracted by fitting a cubic spline to the data. All curves are for  $z = 0$ .

where the  $F_n$  contain dot products of the vectors  $q_i$  and can be generated from recurrence relations [19, 20, 21]. If the initial field is Gaussian the nonlinear power spectrum is then given by

$$P_{NL} = \{P_{11} + P_{13} + P_{15} + \dots\} + \{P_{22} + \dots\} \quad (6)$$

where  $P_{ij} = \langle \delta^{(i)} \delta^{(j)} \rangle$  and  $P_{11} = P_L$ . In what follows, we refer to these groups of terms as the  $P_{1n}$  and  $P_{mn}$  terms respectively. The  $P_{1n}$  terms also arise if we take the cross-spectrum of the initial and evolved fields, while the  $P_{mn}$  terms only arise in the auto-spectrum.

Ignoring combinatorial factors, the  $P_{1n}$  terms are given by

$$P_{1n}(k) \sim P_L(k) \int \prod_{k=1}^{(n-1)/2} [d^3 q_k P_L(q_k)] F_n(\dots) \quad (7)$$

If we factor out the common  $P_L$  and focus on the lowest order correction,  $P_{13}$ , we see that it involves a integral over a single

$P_L$  and a relatively broad kernel which suppresses the oscillations. We expect these terms not to lead to significant out-of-phase contributions, though they can contribute corrections to the damping described above. Since we can isolate these terms by considering the cross-spectrum between the initial and evolved matter fields, we can test the above hypothesis. Table I demonstrates that the shifts in this cross-spectrum are reduced by over an order of magnitude compared to the auto-spectrum and are consistent with zero given our statistical precision. Note that the above argument is only true for the lowest order contribution, but higher order terms are suppressed by additional factors of  $\mathcal{O}(\delta^2)$ , and therefore drop off even more strongly with redshift.

The lowest order  $P_{mn}$  term is

$$P_{22}(k) = \frac{9}{98}Q_1(k) + \frac{3}{7}Q_2(k) + \frac{1}{2}Q_3(k), \quad (8)$$

where the  $Q$ s are defined in Appendix A. In contrast with  $P_{13}$ , these terms (see Eq. A1) involve integrals of products of  $P_L$  which can lead to out-of-phase terms. For example,  $F_2$  is peaked around  $q_1 \approx q_2 \approx k/2$ . When  $P_L$  contains an oscillatory piece, e.g.  $\sin(kr)$ ,  $P_{22}$  contains a piece schematically of the form  $\sin^2(kr/2) \sim 1 + \cos(kr)$ , which oscillates out-of-phase with  $P_L$ . Panel (a) of Fig. 6 explicitly shows this; in fact, this oscillatory part of  $P_{22}$  is very similar to scaled log-derivative of  $P_L$  (Fig. 4; see also [9]). Taylor expanding a shifted power spectrum,

$$P_L(k/\alpha) \simeq P_L(k) - (\alpha - 1) \frac{dP_L}{d \ln k} + \dots \quad (9)$$

we find good agreement between the predicted shift of Fig. 4 and the measured shift in Table I. It is important to note that we have subtracted smooth components for all of these comparisons suggesting that even though perturbation theory does not accurately predict the broad-band shape [16], it does capture the evolution of the acoustic feature.

The above suggests a modified template,

$$P_w(k, \alpha) = \exp\left(-\frac{k^2 \Sigma^2}{2}\right) P_L(k/\alpha) + \exp\left(-\frac{k^2 \Sigma_1^2}{2}\right) P_{22}(k/\alpha). \quad (10)$$

Note that we have damped the oscillations in  $P_{22}$  as for  $P_L$  although we fix the damping scale to the first order calculation. While this damping follows naturally from the heuristic picture described at the start of this section, it is also a consequence of the resummations in eg. Lagrangian perturbation theory. Table I shows that such a template corrects for the shifts observed in the matter.

Looking ahead to biased tracers, we note that one cannot simultaneously fit for the amplitude of the  $P_{22}$  term and the shift, since these are highly degenerate (Eq. 9). Doing so results in highly degraded constraints on the acoustic scale, as is evident in Fig. 5. We need to know the relative amplitude of  $P_{22}$  and  $P_{11}$  to correct the shift. For the mass the relative amplitude is straightforwardly given by perturbation theory. Do the same terms come in for biased tracers and are we able to determine the relative amplitude of the two types of terms?

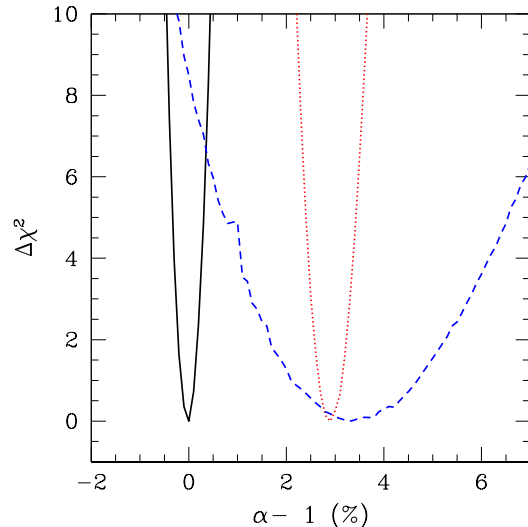


FIG. 5: The  $\Delta\chi^2$  for fits of our  $z = 0$  mass power spectrum to the functional form of Eq. 3 (dashed red), to the form including  $P_{22}$  (solid black) and marginalizing over the amplitude of the  $P_{22}$  term (dashed blue). There are 60 degrees of freedom in the fit, and in each case the best fit is a reasonable fit. Note that Eq. 3 gives a biased acoustic scale, including the  $P_{22}$  term eliminates the bias, and allowing the amplitude of the  $P_{22}$  term to float results in very weak constraints.

## IV. HALOS

### A. Shifts

We investigate the acoustic signal of biased tracers in our simulations by computing the clustering of samples of dark matter halos chosen to lie in narrow mass ranges. Specifically we use the linear theory power spectrum to convert from halo mass to peak height,  $\nu \equiv \delta_c/\sigma(M)$ , and pick halos in the range  $0.85 \leq \nu < 1.15$ ,  $1.15 \leq \nu < 1.45$ ,  $\dots$ . For these we compute both the auto-power spectrum and the cross-power spectra with the linear and evolved dark matter density field. Given the low number density of most of our samples, we focus on the cross-power spectra in the analysis below.

Motivated by the development in the previous section, we test if analogous results exist for halos; Table II and Fig. 3 summarize our findings. We find that (i) the halos exhibit non-zero shifts that are functions of halo type, (ii) the shifts scale approximately as  $D^2$ , and (iii) the shifts are once again absent in the cross-spectrum with the linear density field. As with the matter, this argues that, within the language of perturbation theory, the shifts come from  $P_{mn}$  terms and are dominated by second order corrections. The amplitude of the  $P_{mn}$  terms relative to the  $P_{11}$  terms depends on the type of tracer, to which we now turn.

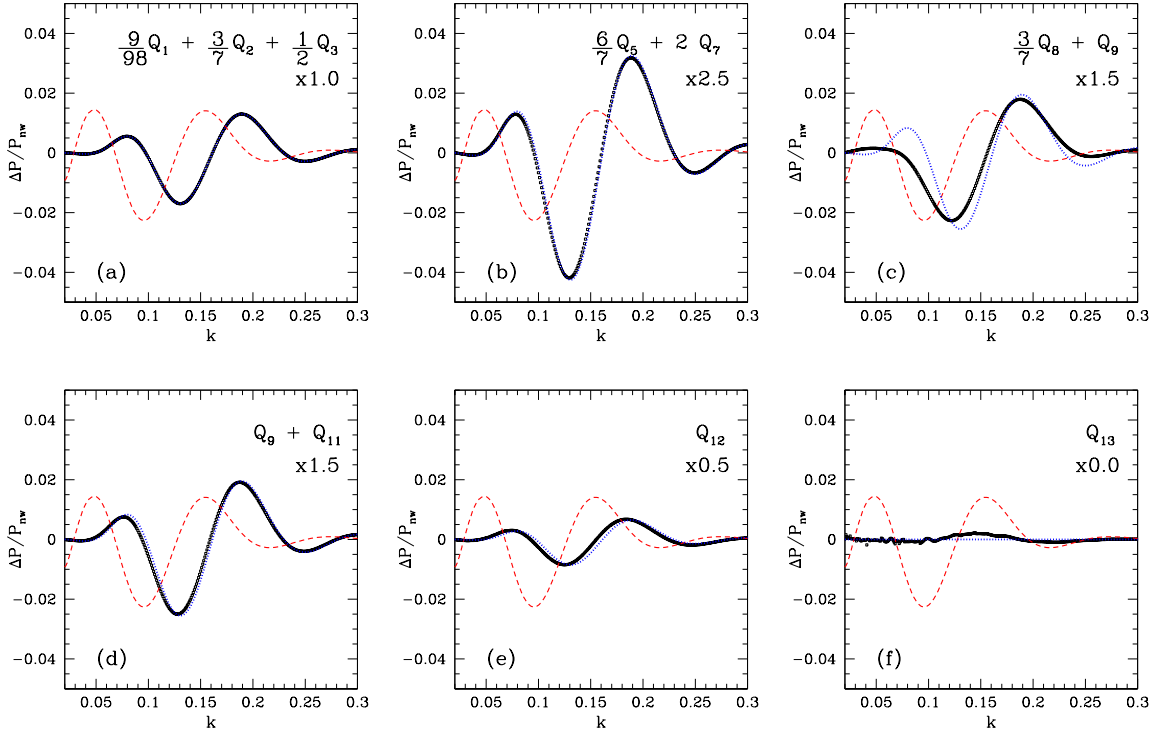


FIG. 6: The six combinations of  $Q_n(k)$ , including the exponential damping (at  $z = 0$ ) that appear in the nonlinear halo power spectrum for  $c$ CDM. For each of these, we subtract a smooth component (by fitting a five point cubic spline), and compare to the “no-wiggle” power spectrum of [4]. The dashed [red] line shows the same procedure applied to the linear power spectrum (divided by 5), while the dotted [blue] line is the  $P_{22}$  correction to the nonlinear matter power (upper left panel). In each panel we have scaled  $P_{22}$  by the multiplicative factor shown to better match each combination of  $Q_n$ .

| $z$ | $\nu = 1.0$      | 1.3              | 1.6              | 1.9              |
|-----|------------------|------------------|------------------|------------------|
| 0.0 | $1.66 \pm 0.19$  | $1.91 \pm 0.33$  | $2.20 \pm 0.36$  | $4.68 \pm 0.51$  |
| 0.3 | -                | $1.38 \pm 0.17$  | $1.53 \pm 0.26$  | $2.39 \pm 0.36$  |
| 0.7 | -                | -                | $0.85 \pm 0.09$  | $1.04 \pm 0.15$  |
| 1.0 | -                | -                | -                | $0.99 \pm 0.17$  |
| 0.0 | $-0.10 \pm 0.06$ | $-0.23 \pm 0.07$ | $-0.16 \pm 0.10$ | $-0.10 \pm 0.12$ |
| 0.3 | -                | $-0.01 \pm 0.06$ | $-0.20 \pm 0.08$ | $0.01 \pm 0.06$  |
| 0.7 | -                | -                | $-0.03 \pm 0.06$ | $-0.10 \pm 0.04$ |
| 1.0 | -                | -                | -                | $-0.04 \pm 0.05$ |
| 0.0 | $-0.01 \pm 0.15$ | $0.12 \pm 0.25$  | $-0.19 \pm 0.26$ | $0.51 \pm 0.31$  |
| 0.3 | -                | $-0.20 \pm 0.11$ | $-0.37 \pm 0.17$ | $-0.58 \pm 0.23$ |
| 0.7 | -                | -                | $-0.27 \pm 0.07$ | $-0.36 \pm 0.10$ |
| 1.0 | -                | -                | -                | $-0.13 \pm 0.11$ |

TABLE II: Shifts in the measured acoustic scale probed by the halo density field as a function of halo peak height and redshift. The first group of numbers are the measured shifts for the halo density field correlated with the matter field, fit with the template of Eq. 3. The second group are for the halo density correlated with the linear density field, again fit with the template of Eq. 3. The final set of numbers are analogous to the first, except fit using the template including the  $P_{mn}$  corrections. Note that the shifts present in the first group are significantly reduced in the other groups.

## B. Eulerian and Lagrangian Bias

We can proceed to develop the perturbation theory of biased tracers in two ways: via Eulerian or Lagrangian perturbation theory. We begin with the former and follow [22] in defining

$$\delta_h = b_1^E \delta + \frac{b_2^E}{2!} \delta^2 + \dots \quad (11)$$

Implicit here is that the halo density is defined in configuration space, and that the density fields have been smoothed on some scale  $R$  to allow us to truncate the expansion. We assume that we are working on scales  $\gg R$ , and will ignore subtleties that arise from the smoothing [23, 24] for now; we explicitly reinstate the smoothing scale in Sec. IV C 2.

The halo auto-power spectrum in Eulerian perturbation theory becomes (see also [23, 24, 25])

$$P_h = (b_1^E)^2 (P_{11} + P_{22}) + b_1^E b_2^E \left( \frac{3}{7} Q_8 + Q_9 \right) + \frac{(b_2^E)^2}{2} Q_{13} + \dots \quad (12)$$

with terms like  $P_{1n}$  included in the missing terms denoted  $\dots$ . The cross spectrum between two tracers  $I$  and  $II$  can be

obtained by the replacements

$$\begin{aligned} b_n &\rightarrow \frac{1}{2} (b_n^{(I)} + b_n^{(II)}) \\ b_n^2 &\rightarrow b_n^{(I)} b_n^{(II)} \\ b_1 b_2 &\rightarrow \frac{1}{2} (b_1^{(I)} b_2^{(II)} + b_1^{(II)} b_2^{(I)}) \end{aligned} \quad (13)$$

As an example, for the cross-spectrum with the mass we obtain

$$P_{h,m} = b_1^E (P_{11} + P_{22}) + \frac{b_1^E b_2^E}{2} \left( \frac{3}{7} Q_8 + Q_9 \right) + \dots \quad (14)$$

Figure 6 shows that the  $P_{22}$  and  $\frac{3}{7}Q_8 + Q_9$  terms contain out-of-phase oscillations with very similar shapes while the  $Q_{13}$  term is essentially non-oscillatory. This suggests that biased tracers will exhibit different shifts than the matter, and the difference will depend on the structure of the bias. It is also worth pointing out that the shift for a  $b_1 \equiv 1$  tracer is *not* the same as for the mass - a fact also evident in Table II where the  $\nu = 1$  halos exhibit different shifts from the matter!

The alternative description is within the Lagrangian picture, which has recently been developed in [26] (see also Appendix B for the basic definitions). Within this formalism the halo auto-spectrum can be written

$$\begin{aligned} P_h = \exp \left[ -\frac{k^2 \Sigma^2}{2} \right] &\left\{ (1 + b_1^L)^2 P_{11} + P_{22} \right. \\ &+ b_1^L \left[ \frac{6}{7} Q_5 + 2Q_7 \right] + b_2^L \left[ \frac{3}{7} Q_8 + Q_9 \right] \\ &+ (b_1^L)^2 [Q_9 + Q_{11}] \\ &\left. + 2b_1^L b_2^L Q_{12} + \frac{1}{2} (b_2^L)^2 Q_{13} \right\} + \dots \end{aligned} \quad (15)$$

where again terms like  $P_{1n}$  have been included in  $\dots$ . As before, expressions for cross-spectra follow from the mapping in Eq. 13, taking care to expand the  $(1 + b_1^L)^2$  term before making the substitutions. Again, Figure 6 shows that the terms which arise look like scaled versions of  $P_{22}$ , except for  $Q_{13}$  which is non-oscillatory.

The structure of these two sets of power spectra appears quite different, especially in the scaling of the different out-of-phase terms with  $b_n$ . However once broad-band power is removed, both of these cases can be effectively written as

$$P_h = \exp \left( -\frac{k^2 \Sigma^2}{2} \right) [\mathcal{B}_1 P_L + \mathcal{B}_2 P_{22}]. \quad (16)$$

where we have implicitly assumed that in both cases some of the higher order terms we have neglected above would sum to an exponential damping, as happens in some variants of both Eulerian and Lagrangian perturbation theory. For the autopower spectra, using the empirically determined scalings in Figure 6, the  $\mathcal{B}$ s are related to the bias parameters by

$$\mathcal{B}_1 = (b_1^E)^2, \quad \mathcal{B}_2 = (b_1^E)^2 + \frac{3}{2} b_1^E b_2^E \quad (17)$$

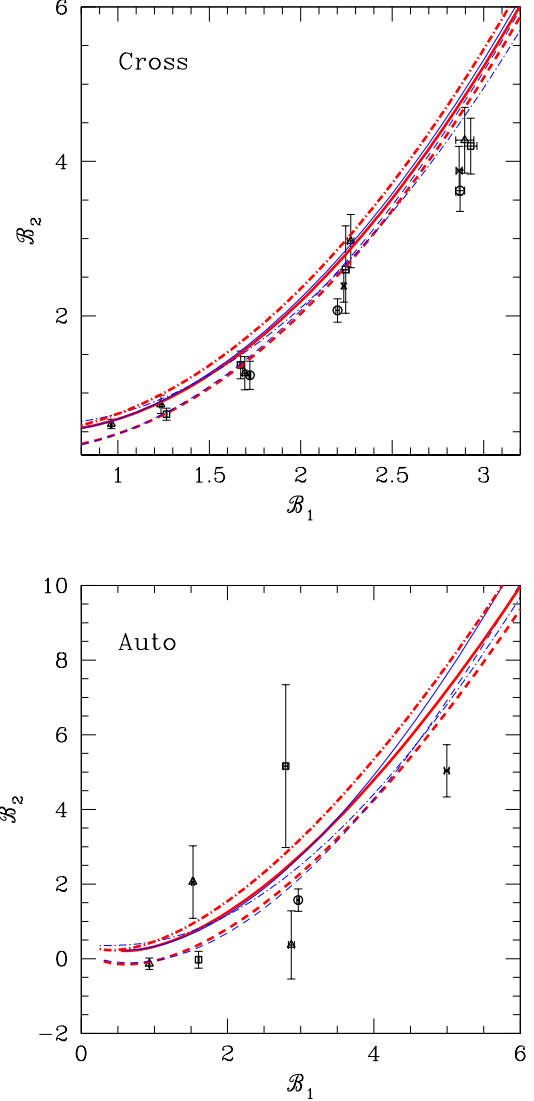


FIG. 7: (Upper) The best fit values of  $\mathcal{B}_1$  and  $\mathcal{B}_2$  for the cross power spectra of halos and the evolved matter density; triangles, squares, circles, and crosses are the  $z = 0, 0.3, 0.7$  and  $1$  data respectively. Note that increasing  $\mathcal{B}_1$  corresponds to increasing  $\nu$ . The solid lines are Sheth-Tormen [15] predictions, while the dashed lines are for Press-Schechter [14]; the thick [red] lines are for Lagrangian theory, while the thin [blue] lines are for Eulerian theory. The dot-dashed lines are based on a quadratic fit to  $b_2(b_1)$ , again both for Eulerian and Lagrangian bias models. The theoretical scatter in these relations is  $\sim 20\%$ . (Lower) As above but for the halo-halo auto-spectrum.

or

$$\begin{aligned} \mathcal{B}_1 &= (1 + b_1^L)^2 \\ \mathcal{B}_2 &= 1 + \frac{5}{2} b_1^L + \frac{3}{2} b_2^L + \frac{3}{2} (b_1^L)^2 + b_1^L b_2^L. \end{aligned} \quad (18)$$

Analogous expressions can be written for the cross-spectra by making the substitutions described above.

If we fit our N-body data to Eq. (16) we find that this form is a good description of the data and the different samples all

lie in a narrow band in the  $\mathcal{B}_1 - \mathcal{B}_2$  plane, as shown in Figure 7 for both the auto- and cross-spectra. This suggests that the halos form a 1-parameter family in terms of the nonlinear bias. This is fortunate, because the ratio of  $\mathcal{B}_2$  to  $\mathcal{B}_1$  is degenerate with the shift of the acoustic scale.

### C. Explaining the Shifts

The previous results simply imply that the amplitude of the shifts is a function of halo bias. However, the perturbative formulation of the previous section also relates the amplitude of the shift to the bias parameters of the halos. We test this relationship here, first using the peak-background split model (see e.g. [15, 27, 28]) and an empirically calibrated  $b_1$ - $b_2$  relationship from simulations.

#### 1. Peak-Background Split

The starting point for the peak-background split is the unconditional multiplicity function

$$\nu f(\nu) d\nu = \frac{M}{2\bar{\rho}} \frac{dn}{dM} dM \quad (19)$$

which can be fit with

$$\nu f(\nu) \propto \left(1 + \frac{1}{(a\nu^2)^p}\right) \left(\frac{a\nu^2}{2}\right)^{1/2} \exp\left(-\frac{a\nu^2}{2}\right) \quad (20)$$

where  $a = 1$ ,  $p = 0$  gives the Press-Schechter mass function [14], while  $a = 0.707$ ,  $p = 0.3$  yields the Sheth-Tormen mass function [15]. Within the assumption of the peak-background split, the conditional multiplicity function is given by the substitution,

$$\nu \rightarrow \nu \left(1 - \frac{\delta}{\delta_c}\right), \quad (21)$$

where  $\delta$  is the background density and  $\delta_c \simeq 1.686$  is the critical overdensity for collapse. The Lagrangian bias parameters then follow from Taylor expanding the (appropriately normalized) conditional multiplicity function as a function of  $\delta$ , yielding  $b_n^L = [\nu f(\nu)]^{-1} d^n / d\delta^n [\nu f(\nu)]$  or

$$b_1^L(\nu) = \frac{1}{\delta_c} \left[ \nu^2 - 1 + \frac{2p}{1 + (a\nu^2)^p} \right], \quad (22)$$

and

$$b_2^L(\nu) = \frac{1}{\delta_c^2} \left[ a^2 \nu^4 - 3a\nu^2 + \frac{2p(2a\nu^2 + 2p - 1)}{1 + (a\nu^2)^p} \right]. \quad (23)$$

The Eulerian bias parameters are then defined by the mapping of the halo density  $\delta_h$  from Lagrangian to Eulerian space,

$$\delta_h^E = (1 + \delta^E)(1 + \delta_h^L) - 1 \quad (24)$$

where the factor of  $(1 + \delta^E)$  comes from the mapping of the Lagrangian to Eulerian volumes. Assuming that the Eulerian

and Lagrangian densities may be related by the Taylor series [28]  $\delta^L = \delta^E + c(\delta^E)^2$  with  $c \simeq -0.805$  assuming spherical collapse, we obtain (see also [29])

$$b_1^E = 1 + b_1^L, \quad (25)$$

and

$$b_2^E = b_2^L + 2b_1^L(1 + c). \quad (26)$$

The theory then makes predictions for both the mass-halo cross-spectrum and the halo-halo auto-spectrum, with the former having significantly less shot noise. Fig. 7 compares these predictions to the observed relation between the  $\mathcal{B}$ s, where we have translated from the bias parameters using the prescription in the previous section. For the cross-spectrum the simple model describes the observed trend with  $\mathcal{B}_1$ , with the differences between the Press-Schechter and Sheth-Tormen predictions being small (and not distinguishable by the data). Both models overpredict  $\mathcal{B}_2$  at high  $\mathcal{B}_1$ . Interestingly, the predictions for the Eulerian and Lagrangian descriptions are virtually indistinguishable, even though the structure of the expressions for the power spectra are very different. For the auto-spectrum we have much more limited N-body data, but again the simple model does an adequate, if not perfect, job of describing what we see.

#### 2. An empirical $b_1 - b_2$ relation

A second approach is to empirically calibrate  $b_1$  and  $b_2$  using models based upon simulations. Recall that in any survey aiming to measure BAO there will be ample data on small scales with which to construct models of the tracers.

The traditional approach to determining the Eulerian bias parameters is to compare various moments of ‘‘counts-in-cells’’ to the perturbative expressions. A concern with such an approach is the effective scale of the measurements, and the validity of the perturbative expressions. An alternative is to compare the auto-spectra of the halos and the mass with the cross-spectrum. The combination of the three spectra can be used to isolate  $b_1$  and  $b_2$ , but this tends to be very noisy and proper shot-noise subtraction is an issue. We outline a different approach below that explicitly only uses large scales; we defer detailed comparisons with other methods to future work.

We start by considering the configuration space statistic

$$\begin{aligned} \mathcal{S}(\mathbf{x}) &= \langle \delta_L^2(\mathbf{x}_1) \delta_h(\mathbf{x}_1) \rangle \\ &= b_1^E \langle \delta_L^2(\mathbf{x}_1) \delta_S(\mathbf{x}_2) \rangle + \frac{b_2^E}{2} \langle \delta_L^2(\mathbf{x}_1) \delta_S^2(\mathbf{x}_2) \rangle, \end{aligned} \quad (27)$$

where  $\mathbf{x} = \mathbf{x}_1 - \mathbf{x}_2$  and  $\delta_S$  is the nonlinear matter density smoothed on a scale  $R$  such that the Eq. 11 is valid. Working to second order in the density field, the second term above reduces to  $b_2 \langle \delta_L(\mathbf{x}_1) \delta_S(\mathbf{x}_2) \rangle^2$ . If we work on large scales  $|\mathbf{x}_1 - \mathbf{x}_2| \gg R$ , then we can approximate the smooth fields by the underlying density field. Fourier transforming, we obtain

$$\mathcal{S}(k) = \frac{b_1^E}{2} \left( \frac{3}{7} Q_8 + Q_9 \right) + b_2^E Q_{13}. \quad (28)$$

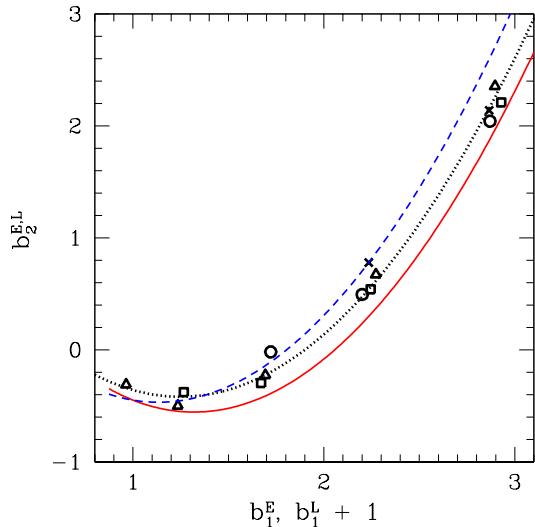


FIG. 8: Measurements of  $b_2$  vs.  $b_1$  for our  $c$ CDM simulations. The symbols are as in Fig. 7. The solid [red] and dashed [blue] lines are the peak-background split predictions for the Lagrangian and Eulerian bias, assuming a Sheth-Tormen [15] mass function. The dotted line is a simple quadratic fit to the data.

The  $k \rightarrow 0$  limit yields a direct measure of  $b_2^E$ ,

$$\mathcal{S}(k \rightarrow 0) = b_2^E Q_{13}(0) \quad (29)$$

where

$$Q_{13}(0) = \int \frac{d^3q}{(2\pi)^3} [P_L(q)]^2 = \int d^3x [\xi_L(x)]^2. \quad (30)$$

Note that these expressions explicitly work at large scales, where the perturbative expansion is valid. While the above derivation was for Eulerian bias, Appendix B shows that the same limit yields

$$\mathcal{S}(k \rightarrow 0) = b_2^L Q_{13}(0) \quad (31)$$

implying that  $b_2^L = b_2^E$ . This is a different relationship than what we obtained within the peak-background split, reflecting the different assumptions made.

The procedure for determining  $b_2^E$  from our simulations are straightforward, except for one subtlety if determining  $\delta_L$  from the initial particle data. Since the initial particle positions are tied to a grid, there is an excess of power at the particle Nyquist frequency, which can alias to lower frequencies when computing  $[\delta_L^2]$ . To avoid this, we smooth the initial density field before squaring; this modifies  $Q_{13}(0)$  to

$$Q_{13,S}(0) = \int \frac{d^3q}{(2\pi)^3} [P_L(q)W(q)]^2, \quad (32)$$

where  $W(q)$  is the Fourier transform of the smoothing kernel (we adopt a Gaussian of comoving width  $5 h^{-1} \text{Mpc}$ ). We then determine  $b_2$  by fitting the  $\mathcal{S}(k)$  measurements below  $k <$

$0.05 h \text{Mpc}^{-1}$  to Eq. 28 where  $b_1^E$  is determined from the low  $k$  limit of the halo-linear density cross correlation.

Fig. 8 shows the measured bias parameters for our  $c$ CDM simulations, compared with the Eulerian and Lagrangian predictions. Fig. 7 demonstrates that the observed relationship well describes the observed  $\mathcal{B}_1 - \mathcal{B}_2$  correlation, and therefore shifts in the acoustic scale. It is important to emphasize these constraints on  $b_2$  are independent of the acoustic oscillations. In fact, the  $b_2$  constraint depends on the  $Q_{13}$  contribution to the power spectrum, which is irrelevant for BAO.

In principle higher order measures or the observed clustering on small(er) scales contain information about  $\mathcal{B}_i$  for the sample of interest, and we have shown that improving our ability to model the higher order terms could bear dividends. Testing such methods is beyond our scope here, and we defer it to future work.

#### D. Shifts, Corrected - A Template for Halos

We are now in a position to construct a template for the BAO feature traced by halos. The key ingredient is a calibrated  $\mathcal{B}_1 - \mathcal{B}_2$  relationship; we assume the Sheth-Tormen form of Eulerian peaks-bias here. Assuming an estimate of the large-scale bias, this fixes  $\mathcal{B}_2/\mathcal{B}_1$ . We fit the observed power spectrum to

$$P_w(k, \alpha) = b_1 \left[ \exp\left(-\frac{k^2 \Sigma^2}{2}\right) P_L(k/\alpha) + \exp\left(-\frac{k^2 \Sigma_1^2}{2}\right) \frac{\mathcal{B}_2}{\mathcal{B}_1} P_{22}(k/\alpha) \right] \quad (33)$$

where  $b_1$  and  $\Sigma$  are fit parameters,  $\Sigma_1$  is determined from linear perturbation theory (Eq. 2).

We show that this procedure returns (almost) unbiased estimates of the acoustic scale in Table II. These results come from the halo-mass cross-spectrum, which is significantly better determined than the halo auto-correlation function. The results from the auto-correlation function are consistent with the shift being corrected, but the errors are too large to allow a meaningful constraint with the simulations we have. In principle one could obtain even more accurate constraints by modeling each of the perturbation theory terms separately, but this becomes more model dependent so we don't pursue this line here.

These results allow us to identify sources of systematic errors in the BAO measurement and estimate their level. However, before doing so, we first extend our results from  $c$ CDM to  $\Lambda$ CDM.

#### V. IMPLICATIONS FOR $\Lambda$ CDM

In order to extend the results of the previous sections to a  $\Lambda$ CDM cosmology, it is useful to summarize the various components of our model and see how they generalize to a different cosmology.

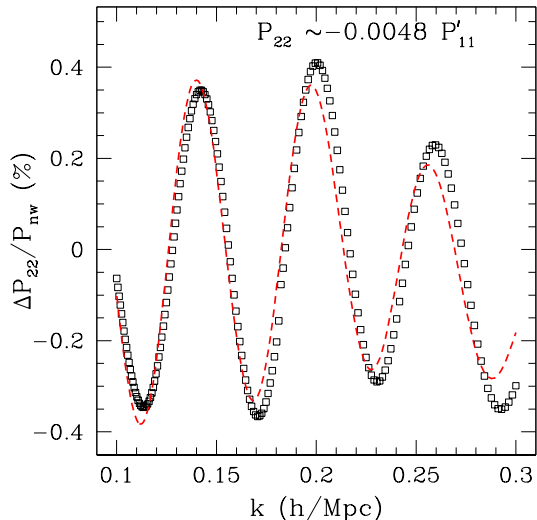


FIG. 9: As in Fig. 4, except for  $\Lambda$ CDM.

- The shifts in the matter were caused by the  $P_{22}$  piece of the power spectrum, which well approximated a scaled derivative of the linear power spectrum (after subtracting out the broad-band shape). The scaling was directly interpretable as the shift in the acoustic scale. Fig. 9 shows that this continues to hold for  $\Lambda$ CDM, with the  $z = 0$  shift predicted to be  $\sim 0.5\%$ , in agreement with simulation results by [12] and analytic arguments by [9, 30].
- Extending these results to biased tracers generated additional shifts, sourced by terms whose oscillatory components resembled scaled versions of  $P_{22}$ . This continues to be true in  $\Lambda$ CDM with exactly the same scalings of  $P_{22}$ ; Fig. 10 shows an example. This implies that the template of Eq. 33 as well as the relationship between the  $\mathcal{B}_m$  and the bias parameters  $b_n$  continues to hold for  $\Lambda$ CDM.
- The final component was to demonstrate that simple models of halo bias indeed explained the resulting shifts. The first of these - a peaks-bias model - is manifestly cosmology independent. The second attempted to empirically calibrate the bias parameters; Fig. 11 shows a similar calibration for  $\Lambda$ CDM. Interestingly, we find a similar cosmology independence for the empirical calibrations, manifested in both the comparisons with  $c$ CDM and with the different redshifts for  $\Lambda$ CDM.
- The above allows us to predict that for  $\Lambda$ CDM the shift is roughly an order of magnitude smaller than  $c$ CDM and is given by  $\alpha - 1 \sim 0.5\% \times D^2 \times \mathcal{B}_2/\mathcal{B}_1$ .

We can now turn to the systematic error budget for BAO. The expression above gives the bias in the acoustic scale if one ignored the effects in this paper. Errors in the calibration of  $\mathcal{B}_2/\mathcal{B}_1$  directly translate into an error in the acoustic scale;

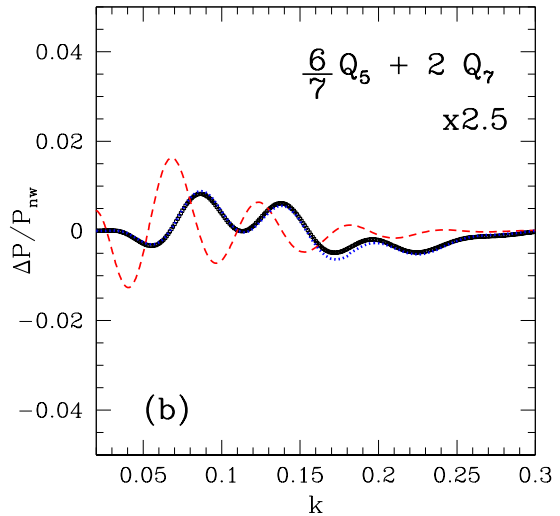


FIG. 10: An example of the out-of-phase components, as in Fig. 6, except for a  $\Lambda$ CDM cosmology. Note the reduced amplitude of the  $P_{mn}$  terms, indicating smaller shifts than for our toy cosmology. We also note that the factors that scale  $P_{22}$  to the other  $Q_n$  combinations appear to be independent of the underlying cosmology.

eg. a 20% error in  $\mathcal{B}_2/\mathcal{B}_1$  (approximately how good our toy models are) would correspond to a bias of  $0.1\% \times D^2$ .

Our analysis also demonstrates that the degree of shift is sensitive to the degree of nonlinearity, or amplitude of the power spectrum. The out-of-phase terms scale as one higher power of  $P_L$  than the linear terms. To the extent that the amplitude is degenerate with a change in bias of the tracer, uncertainty in the amplitude leads to uncertainty in the shift. As an example, if the local slope of the  $\mathcal{B}_2 - \mathcal{B}_1$  relation is  $\beta$  and we imagine holding the large-scale power fixed, a change in the amplitude  $\delta P_L/P_L = \varepsilon$  will induce a change  $\delta \mathcal{B}_1/\mathcal{B}_1 = -\varepsilon$  and  $(2 - \beta)\varepsilon$  in the  $P_{22}$  term in Eq. (16). From Fig. 7 we see typical values of  $\beta \sim 1$ . Applying the same scaling between  $\alpha$  and  $P_{22}$  as above this would lead to a shift in the acoustic scale of  $\sim 0.005 \varepsilon$  for  $\Lambda$ CDM. Thus 10% knowledge of the amplitude of  $P_L$  would give  $< 0.1\%$  uncertainty in  $\alpha$ .

Fig. 12 summarizes the systematic error budget, and compares it to the observational error goals for Stage III and Stage IV experiments [31]. None of these systematics are expected to be relevant for Stage III experiments, and are within a factor of a few of the requirements for Stage IV experiments.

## VI. GALAXIES

The above results have focused on the case of halo samples of a single mass, but can be generalized to arbitrary combinations of halo samples. Of particular interest is the halo model for galaxies (for a review, see [32]), that has been very successful in describing the large scale clustering of galaxies.

The halo model assumes that all galaxies live in dark matter halos and the probability of a particular galaxy occupying

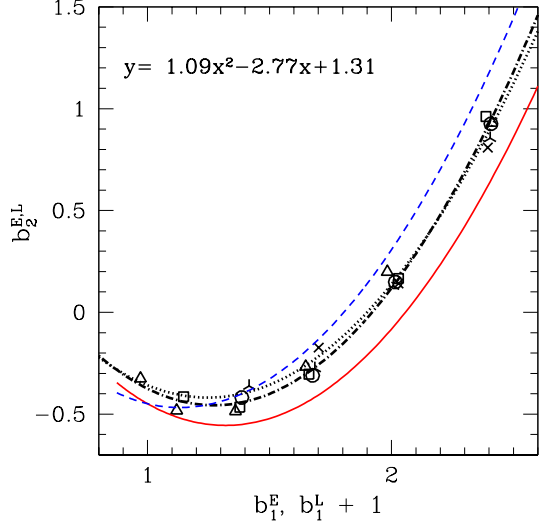


FIG. 11: As in Fig. 8, except for  $\Lambda$ CDM. These measurements were based on an additional set of simulations employing  $1200^3$  particles in cubic boxes of side  $1250 h^{-1}$  Mpc. The symbols - triangles, squares, circles, stars and crosses correspond to  $z = 0, 0.3, 0.5, 0.7$  and  $1.0$  respectively. The dotted line shows the fit from Fig. 8 while the dot-dashed line is the quadratic fit in the inset.

a given halo depends only on the halo mass. Under this assumption the large scale clustering of galaxies is determined by the clustering of the halos, weighted by the mean number of galaxies in each halo. If we denote the mean number of galaxies in a halo of mass  $M$  as  $N(M)$ , the galaxy power spectrum is

$$P_{\text{gal}} = \frac{\sum_{i,j}^n w_i w_j P_h^{i,j}}{(\sum_i^n w_i)^2}, \quad (34)$$

where  $P_h^{i,j}$  is the halo cross-spectrum for masses  $i$  and  $j$  and the weights are determined by the halo mass function,  $n_h(M)$ , and  $N(M)$  via

$$w_i = n_h(M_i) N(M_i) \Delta M_i \quad (35)$$

Substituting Eq. 16 for the halo power spectrum and noting that the exponential damping is (to a good approximation) independent of halo mass, we find that  $P_{\text{gal}}$  retains the same structure,

$$P_{\text{gal}}(k) = \exp\left(-\frac{k^2 \Sigma^2}{2}\right) [\mathcal{B}_{1,\text{gal}} P_L + \mathcal{B}_{2,\text{gal}} P_{22}]. \quad (36)$$

but with new coefficients

$$\mathcal{B}_{n,\text{gal}} = \frac{1}{\mathcal{N}^2} \int dM_1 n_h(M_1) N(M_1) \times \int dM_2 n_h(M_2) N(M_2) \mathcal{B}_n(M_1, M_2), \quad (37)$$

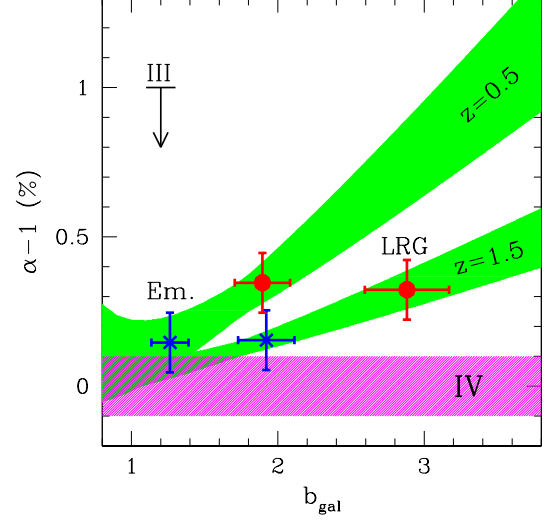


FIG. 12: Estimates of the shift (if not corrected) as a function of halo bias and redshift for our  $\Lambda$ CDM cosmology. The width of the shaded regions denotes the error estimated from the difference between the Press-Schechter and Sheth-Tormen forms in the conversion between  $\mathcal{B}_1$  and  $\mathcal{B}_2/\mathcal{B}_1$  and demonstrates approximately how errors in the theory propagate into a residual shift. We highlight two example populations of halos: a  $b(z=0) = 1$  sample [blue crosses] to represent emission line galaxies, and a  $b(z=0) = 1.5$  sample [red circles] to represent an elliptical sample. In both cases, the clustering of the sample is assumed to be constant with redshift. The errorbars correspond to a 10% measurement of the bias. Also shown are nominal distance accuracies for Stage III (currently underway) and Stage IV (future) experiments.

where the normalizing factor

$$\mathcal{N} = \int dM n_h(M) N(M) \quad (38)$$

is just the mean number of galaxies. Then, assuming  $\mathcal{B}_n(M_1, M_2)$  factorizes (or is a sum of factorizable pieces), we can simply replace  $b_n$  in our earlier expressions with

$$b_{n,\text{gal}} = \frac{1}{\mathcal{N}} \int dM n_h(M) N(M) b_n(M) \quad (39)$$

Note that, as expected,  $\mathcal{B}_{1,\text{gal}}$  simplifies to  $b_{\text{gal}}^2$  where the galaxy bias  $b_{\text{gal}}$  is just the weighted sum of the halo  $b_1$ 's. The expressions for cross-spectra of galaxy samples follow a similar pattern to the halo cross spectra discussed earlier (Eq. 13).

For a concrete example, we assume a  $N(M)$  of the form,

$$N(M) = \Theta(M - M_{\text{min}}) [1 + M/M_1]. \quad (40)$$

We consider two cases:  $M_1 = \infty$  or a “threshold” sample, and  $M_1 = 10M_{\text{min}}$  or a “satellite” sample; Fig. 13 plots the shifts as we vary  $M_{\text{min}}$  from  $10^{12} h^{-1} M_{\odot}$  upwards. As one might expect, the increased weighting towards higher halo masses increases the shifts, although they remain smaller than the required systematics levels for near future surveys. The

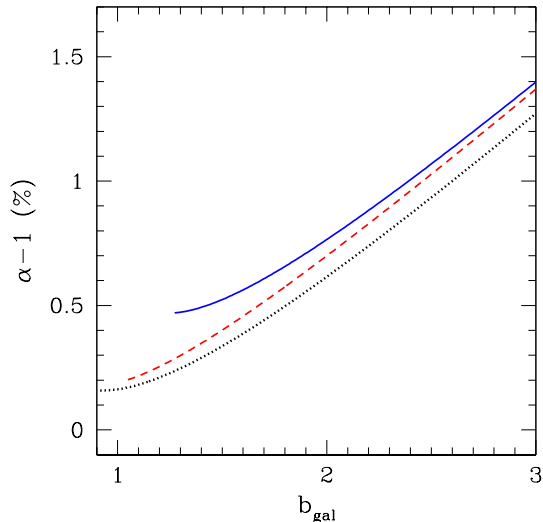


FIG. 13: The shifts for three example galaxy samples at  $z = 0$  for  $\Lambda$ CDM, as a function of the galaxy bias. The dotted line shows the shifts for halos, while the dashed [red] and solid [blue] lines are for threshold and satellite samples respectively (see the text for more details). We assume the Eulerian Sheth-Tormen peaks-bias model for definiteness.

above also suggests that one could control systematics by re-weighting galaxies, the details of which will, of course, be population dependent.

## VII. REDSHIFT SPACE

Until now, everything we have done has been in real space, ignoring the redshift space distortions that arise from peculiar velocities. The Lagrangian perturbation theory formalism allows us to predict the effect of large-scale redshift space distortions in a straightforward manner, although the comparison with simulations is made more difficult and additional modeling of the observations is required. We defer a detailed comparison with simulations to future work, but comment on the trends here.

The power spectrum now becomes anisotropic,  $P(k, \mu)$ , with  $\mu$  the cosine of the angle between the line-of-sight and  $k$  and our previous results correspond to  $\mu = 0$ . Including the full  $\mu$  dependence results in different combinations of  $Q_n$  entering the expression. Some of these are in phase with  $P_L$ , while some are out of phase. This means the shifts in redshift space will be different than those in real space, as seen in simulations (e.g. [12]). The in-phase term ( $E_{12}$ , see Eq. A73 in [26]) is much smaller than  $P_L$ , and we ignore it for now.

If we concentrate on the isotropic piece of the power spectrum [33], we again find that the remaining combinations of  $Q_n$  which enter are proportional to  $P_{22}$  and the constants of proportionality appear to cosmology independent (though they do depend additionally on  $f \equiv d \ln D / d \ln a \simeq \Omega^{0.6}$ ).

There are no new degrees of freedom introduced theoretically, so in principle the redshift space shifts are determined from the same modeling as the real space shifts discussed previously.

For  $\Lambda$ CDM at  $z = 0$  the predicted shift in the matter grows from 0.5% to 0.75%, consistent with the shifts seen in [12]. For biased tracers, the effect is to increase the shift by an  $f$ -dependent (but roughly bias-independent) constant. For  $f = 1$  (corresponding to high  $z$ ), this constant is  $\sim 0.5\% D^2$ , while for  $f \sim 0.5$  (corresponding to  $z \sim 0$ ), it is  $\sim 0.3\%$ . If uncorrected, these shifts could be relevant for future experiments; we leave detailed calibrations to future work.

## VIII. DISCUSSION

The propagation of acoustic waves in the early universe provides a robust means for determining the expansion history of the Universe, and constraining cosmology. The standard ruler is calibrated in the linear regime by observations of the CMB, but observed today with biased, nonlinear tracers. Since the acoustic scale is so large, the effects of bias and nonlinearity on the acoustic scale is small, but future experiments may have enough sensitivity that it needs to be taken into account. We have begun this program here.

Using a set of N-body simulations of an extreme cosmology, in which the acoustic scale is relatively small and the nonlinearity quite pronounced, we have shown that shifts in the scale grow quadratically with the amplitude of the linear theory power spectrum for both the mass and for dark matter halos. Motivated by this, and guided by arguments from Eulerian and Lagrangian perturbation theory, we found the dominant second-order contribution to the peak shift. This contribution,  $P_{22}$ , quite well approximates the derivative of the acoustic signal, explaining why it leads to a peak shift and allowing us to estimate how the amplitude of the  $P_{22}$  term can be translated into a shift in the fitted acoustic scale.

For dark matter halos the contribution depends on two bias parameters,  $b_1$  and  $b_2$ , allowing in principle arbitrary shifts of the acoustic scale. We showed however that dark matter halos, which will be the hosts of any galaxies we observe, obey a relation between  $b_1$  and  $b_2$  which is relatively well predicted by the peak-background split. Once these two terms are related the acoustic scale for nonlinear, biased tracers can be accurately determined, allowing high fidelity measurements of distances using baryon acoustic oscillations.

We have described how redshift space distortions affect the scale shifts within the context of Lagrangian perturbation theory, where they increase the shift by tens of percent at low  $z$  and about a factor of 2 at high  $z$ .

In this paper we have concentrated on the effects of nonlinear gravitational evolution and halo biasing, showing that these effects could be understood at the 0.1% level. At this level of precision the inclusion of additional physics, such as differential evolution of the baryonic and dark matter components or the details of galaxy formation, may enter and investigations in this direction should be undertaken. We have also assumed that the linear theory template is perfectly under-

stood, which also deserves further study. Such investigations must be part of any future high-precision BAO experiment.

The simulations presented in this paper were carried out using computing resources of the National Energy Research Scientific Computing Center and the Laboratory Research Computing project at Lawrence Berkeley National Laboratory. NP is supported by NASA HST-HF-01200.01 and LBNL. MW is supported by NASA and the DoE. This research was additionally supported by the Laboratory Directed Research and Development program at Lawrence Berkeley National Laboratory, and by the Director, Office of Science, of the U.S. Department of Energy under Contract No. DE-AC02-05CH11231.

#### APPENDIX A: EXPRESSIONS FOR $P_{mn}$ FOR $m = 2, n = 2$

The expressions for  $P_{mn}$  for a biased tracer (in both Eulerian and Lagrangian perturbation theory) can be simply written by defining [26]

$$Q_n(k) = \frac{k^3}{4\pi^2} \int_0^\infty dr P_L(kr) \int_{-1}^1 dx P_L(k\sqrt{y}) \tilde{Q}_n(r, x), \quad (\text{A1})$$

where  $y(r, x) = 1 + r^2 - 2rx$ ,  $P_L$  is the linear power spectrum and the  $\tilde{Q}_n$  are given by

$$\begin{aligned} \tilde{Q}_1 &= \frac{r^2(1-x^2)^2}{y^2}, & \tilde{Q}_2 &= \frac{(1-x^2)rx(1-rx)}{y^2}, \\ \tilde{Q}_3 &= \frac{x^2(1-rx)^2}{y^2}, & \tilde{Q}_4 &= \frac{1-x^2}{y^2}, \\ \tilde{Q}_5 &= \frac{rx(1-x^2)}{y}, & \tilde{Q}_6 &= \frac{(1-3rx)(1-x^2)}{y}, \\ \tilde{Q}_7 &= \frac{x^2(1-rx)}{y}, & \tilde{Q}_8 &= \frac{r^2(1-x^2)}{y}, \\ \tilde{Q}_9 &= \frac{rx(1-rx)}{y}, & \tilde{Q}_{10} &= 1-x^2, \\ \tilde{Q}_{11} &= x^2, & \tilde{Q}_{12} &= rx, & \tilde{Q}_{13} &= r^2 \end{aligned}$$

#### APPENDIX B: COMPUTING $\langle \delta_L^n \delta_{\text{obj}} \rangle$ IN RESUMMED LPT

We present expressions for evaluating  $\langle [\delta_L^n] \delta_{\text{obj}} \rangle$  in resummed Lagrangian perturbation theory, where  $\delta_{\text{obj}}$  is the density field of biased tracers. These expressions follow [26] and we refer the reader there for detailed calculations.

The density field for a biased tracer can be defined by the displacement field  $\Psi(\mathbf{q})$  and a function of the smoothed initial density field in Lagrangian space,  $F[\delta_L(\mathbf{q})]$ , as

$$\delta_{\text{obj}}(\mathbf{x}) = \int d^3q F[\delta_L(\mathbf{q})] \delta_D^{(3)}(\mathbf{x} - \mathbf{q} - \Psi), \quad (\text{B1})$$

where  $\mathbf{x}$  and  $\mathbf{q}$  are the Eulerian and Lagrangian positions and  $\delta_D^{(3)}$  is the 3D Dirac  $\delta$  function. We implicitly assume that the argument to  $F$  has been smoothed on some scale much smaller than the large scales of relevance here, allowing us to ignore the smoothing here (see [26] for a detailed justification). We cross correlate this with a field defined by  $\exp(i\lambda\delta_L)$ ;  $\delta_L^n$  is then simply obtained by taking the  $n$ -th derivative with respect to  $\lambda$  and setting  $\lambda$  to zero.

The cross-power spectrum of the two fields is then given by (compare to Eq. 9 of [26])

$$\mathcal{H}(k) = \int d^3q e^{-i\mathbf{k}\mathbf{q}} \left[ \int_{-\infty}^{\infty} \frac{d\lambda_2}{2\pi} \tilde{F}(\lambda_2) \times \left\langle e^{i(\lambda_1\delta_L(\mathbf{q}_1) + \lambda_2\delta_L(\mathbf{q}_2) + i\mathbf{k}\Psi(\mathbf{q}_2))} \right\rangle \right], \quad (\text{B2})$$

where  $\mathbf{q} = \mathbf{q}_1 - \mathbf{q}_2$  and  $\tilde{F}$  is the Fourier transform of  $F$ . The correlators of interest are then given by

$$\langle [\delta_L^n] \delta_{\text{obj}} \rangle = \frac{1}{i^n} \frac{d^n \mathcal{H}}{d\lambda_1^n} \Big|_{\lambda_1=0}. \quad (\text{B3})$$

The algebra now follows through as in [26] using the cumulant expansion theorem, and collecting all zero-lag correlators to yield (compare to Eq. 24 in [26]),

$$\begin{aligned} \mathcal{H}(k) &= \exp \left[ \sum_{m=1}^{\infty} \frac{(-1)^m}{(2m)!} B_{0\ 2m}^{00}(\mathbf{k}, \mathbf{q}) \right] \int d^3q e^{-i\mathbf{k}\mathbf{q}} \int_{-\infty}^{\infty} \frac{d\lambda_2}{2\pi} \tilde{F}(\lambda_2) \times \\ &e^{-\lambda_1^2\sigma^2/2 - \lambda_2^2\sigma^2/2} \exp \left[ -\lambda_1\lambda_2\xi(|\mathbf{q}|) + \sum_{n_1+n_2 \geq 1} \sum_{m_2 \geq 1} \frac{i^{n_1+n_2+m_2}}{n_1!n_2!m_2!} \lambda_1^{n_1} \lambda_2^{n_2} B_{0\ m_2}^{n_1\ n_2}(\mathbf{k}, \mathbf{q}) \right] \end{aligned} \quad (\text{B4})$$

where

$$\xi(|\mathbf{q}|) = \langle \delta_L(\mathbf{q}_1) \delta_L(\mathbf{q}_2) \rangle; \quad \sigma^2 = \xi(0), \quad (\text{B5})$$

and

$$B_{0\ m_2}^{n_1\ n_2} \equiv \langle [\delta_L(\mathbf{q}_1)]^{n_1} [\delta_L(\mathbf{q}_1)]^{n_2} [\mathbf{k}\Psi(\mathbf{q}_2)]^{m_2} \rangle_c, \quad (\text{B6})$$

with  $\langle \dots \rangle_c$  denoting the connected moments.

Given Eq. B4, it is straightforward (if tedious) to compute expressions for the correlators in Eq. B3. Of particular interest to us here is the  $k \rightarrow 0$  limit of  $\langle [\delta_L^2] \delta_{\text{obj}} \rangle$  which, as in Eulerian perturbation theory, is given by

$$S(k \rightarrow 0) = b_2^L Q_{13}(0), \quad (\text{B7})$$

with  $b_2^L$  defined by

$$\begin{aligned} b_n^L &\equiv \int_{-\infty}^{\infty} \frac{d\lambda}{2\pi} e^{-\lambda^2 \sigma^2 / 2} \tilde{F}(\lambda) (i\lambda)^n \\ &= \frac{1}{\sqrt{2\pi}\sigma} \int_{-\infty}^{\infty} d\delta e^{-\delta^2 / 2\sigma^2} \frac{d^n F}{d\delta^n} \end{aligned} \quad (\text{B8})$$

this  $k \rightarrow 0$  limit can be obtained more simply by dropping the  $\mathbf{k} \cdot \Psi$  term in Eq. B2, leaving only Gaussian fields in the exponent. These fields have only a second connected moment, thus only the  $\lambda_1 \lambda_2 \xi(|\mathbf{q}|)$  term survives in the last exponential of Eq. B4 and expanding this exponential gives Eq. B7.

While the full formalism is required in general, we note that

- 
- [1] P. J. E. Peebles and J. T. Yu, *Astrophys. J.* **162**, 815 (1970).
  - [2] R. A. Sunyaev and Y. B. Zeldovich, *Astrophys. Space Sci.* **7**, 3 (1970).
  - [3] A. G. Doroshkevich, Y. B. Zel'Dovich, and R. A. Sunyaev, *Soviet Astronomy* **22**, 523 (1978).
  - [4] D. J. Eisenstein and W. Hu, *Astrophys. J.* **496**, 605 (1998), arXiv:astro-ph/9709112.
  - [5] A. Meiksin, M. White, and J. A. Peacock, *Mon. Not. R. Astron. Soc.* **304**, 851 (1999), arXiv:astro-ph/9812214.
  - [6] D. J. Eisenstein, H.-J. Seo, and M. White, *Astrophys. J.* **664**, 660 (2007), arXiv:astro-ph/0604361.
  - [7] S. Bharadwaj, *Astrophys. J.* **460**, 28 (1996), arXiv:astro-ph/9511085.
  - [8] S. Bharadwaj, *Astrophys. J.* **472**, 1 (1996), arXiv:astro-ph/9606121.
  - [9] M. Crocce and R. Scoccimarro, *Phys. Rev. D* **77**, 023533 (2008), 0704.2783.
  - [10] T. Matsubara, *Phys. Rev. D* **77**, 063530 (2008), 0711.2521.
  - [11] R. E. Smith, R. Scoccimarro, and R. K. Sheth, *Phys. Rev. D* **77**, 043525 (2008), arXiv:astro-ph/0703620.
  - [12] H.-J. Seo, E. R. Siegel, D. J. Eisenstein, and M. White, *Astrophys. J.* accepted (2008), arXiv:0805.0117.
  - [13] N. Padmanabhan, M. White, and J. D. Cohn, *ArXiv e-prints* (2008), 0812.2905.
  - [14] W. H. Press and P. Schechter, *Astrophys. J.* **187**, 425 (1974).
  - [15] R. K. Sheth and G. Tormen, *Mon. Not. R. Astron. Soc.* **308**, 119 (1999), arXiv:astro-ph/9901122.
  - [16] J. Carlson, M. White, and N. Padmanabhan, *ArXiv e-prints* (2009), 0905.0479.
  - [17] M. White, *Astrophys. J. Supp.* **143**, 241 (2002), arXiv:astro-ph/0207185.
  - [18] M. Davis, G. Efstathiou, C. S. Frenk, and S. D. M. White, *Astrophys. J.* **292**, 371 (1985).
  - [19] M. H. Goroff, B. Grinstein, S.-J. Rey, and M. B. Wise, *Astrophys. J.* **311**, 6 (1986).
  - [20] N. Makino, M. Sasaki, and Y. Suto, *Phys. Rev. D* **46**, 585 (1992).
  - [21] B. Jain and E. Bertschinger, *Astrophys. J.* **431**, 495 (1994), arXiv:astro-ph/9311070.
  - [22] J. N. Fry and E. Gaztanaga, *Astrophys. J.* **413**, 447 (1993), arXiv:astro-ph/9302009.
  - [23] A. F. Heavens, S. Matarrese, and L. Verde, *Mon. Not. R. Astron. Soc.* **301**, 797 (1998), arXiv:astro-ph/9808016.
  - [24] P. McDonald, *Phys. Rev. D* **74**, 103512 (2006), arXiv:astro-ph/0609413.
  - [25] R. E. Smith, R. Scoccimarro, and R. K. Sheth, *Phys. Rev. D* **75**, 063512 (2007), arXiv:astro-ph/0609547.
  - [26] T. Matsubara, *Phys. Rev. D* **78**, 083519 (2008), arXiv:0807.1733.
  - [27] S. Cole and N. Kaiser, *Mon. Not. R. Astron. Soc.* **237**, 1127 (1989).
  - [28] H. J. Mo and S. D. M. White, *Mon. Not. R. Astron. Soc.* **282**, 347 (1996), arXiv:astro-ph/9512127.
  - [29] R. Scoccimarro, R. K. Sheth, L. Hui, and B. Jain, *Astrophys. J.* **546**, 20 (2001), arXiv:astro-ph/0006319.
  - [30] A. Taruya, T. Nishimichi, S. Saito, and T. Hiramatsu, *ArXiv e-prints* (2009), 0906.0507.
  - [31] A. Albrecht, G. Bernstein, R. Cahn, W. L. Freedman, J. Hewitt, W. Hu, J. Huth, M. Kamionkowski, E. W. Kolb, L. Knox, et al., *ArXiv Astrophysics e-prints* (2006), arXiv:astro-ph/0609591.
  - [32] A. Cooray and R. Sheth, *Physics Reports* **372**, 1 (2002), arXiv:astro-ph/0206508.
  - [33] N. Padmanabhan and M. White, *Phys. Rev. D* **77**, 123540 (2008), 0804.0799.